Optimal Split Ratio in Small High Speed PM Machines Considering Both Stator and Rotor Loss Limitations

J. Ma, and Z.Q. Zhu, *Fellow, IEEE*
(Invited)

***Abstract*—The split ratio which is defined as the ratio between rotor and stator outer diameters is critical for permanent magnet (PM) machines. In this paper, the split ratio in small high speed PM machines is optimized analytically by considering both stator and rotor loss limitations. By this way, the thermal constrains in both stator and rotor parts can be taken into account. It shows that both losses can significantly affect the optimal split ratio and the machine performance. By considering the influence of rotor losses, especially the rotor eddy current loss, the optimal split ratio is increased significantly in certain scenarios. The output torque is calculated analytically and the influences of several key design parameters on the optimal split ratio, i.e. slot/pole combinations and magnet materials, are also investigated in details. Finally, finite element (FE) analyses are carried out for validating of the analytical model.**

***Index Terms*—High speed, permanent magnet, split ratio.**

I. INTRODUCTION

HIGH speed permanent magnet machines have been applied widely nowadays due to their advantages such as high power density, small volume and low weight, etc. [1]-[4]. As one of the most important design parameters, the split ratio, which is defined as the ratio between the outer diameters of rotor and stator, has a significant influence on the torque density, efficiency and cost [5].

There are many discussions about the optimal split ratio of PM machines. In [6], it shows that the optimal split ratio exists for the minimum winding copper loss, and it affects the magnetic circuit significantly. The optimal split ratio for motors having different drive modes and winding configurations is investigated in [7], in which the influence of detailed design parameters, e.g. tooth tip heights, end windings, etc., are also taken into account. The analytical models for the optimal split ratio of machines having inner and outer rotors are derived in [8]-[9], and the split ratio is optimized in fractional slot interior permanent magnet (IPM) machines in [10].Previous literatures mainly focus on the low speed machine. In contrast, [11]-[12] investigate the optimal split ratio in high speed PM machines with brushless DC (BLDC) drive mode.

Manuscript was submitted for review on 20, January, 2019.

J. Ma and Z. Q. Zhu are with the Department of Electrical and Electronic Engineering, The University of Sheffield, Sheffield, S1 3JD, U.K. (e-mail: jma19@sheffield.ac.uk, z.q.zhu@sheffield.ac.uk).

Digital Object Identifier 10.30941/CESTEMS.2019.00002

The influences of iron loss, copper loss and the airgap length are also studied in details. It shows that the optimal split ratio decreases measurably when the iron loss is considered. In addition, the increased airgap length enhances the optimal split ratio in high speed PM machines due to the decreased iron loss. The split ratio of high speed PM machines is optimized based on the lumped parameter thermal model in [13]. The winding temperature rise is considered as the limitation, and the effects of copper loss, iron loss and windage loss are taken into account. The optimal split ratio is also analytically determined in [14] and [15], which account for the iron loss in the split ratio optimization directly. In addition, the influence of several key design parameters are also investigated in these two papers, e.g. airgap lengths and rotor pole pairs, etc.

However, the rotor losses, especially the rotor eddy current loss is almost neglected in the previous literatures. Since these papers mainly focus on relatively large machines, and they assume the rotor eddy current loss can be effectively reduced by using manufacture techniques, e.g. PM segmentations. Nevertheless, the rotor employing a magnet ring and a nonmagnetic sleeve is usually adopted in small high speed PM machines due to its easy manufacture process, as stated in many literatures and applied widely in industry applications [16]-[19]. As a result, the segmentation can be hardly used in high speed PM machines with small sizes, which means the influence of rotor eddy loss is consequently much more significant and should be considered.

In this paper, the split ratio in small high speed PM machines is optimized by a newly proposed simple method. Both stator and rotor loss limitations are calculated based on thermal considerations and merged into the optimization process. The influence of several key design parameters, e.g. slot/pole combinations and magnet materials, are also investigated in detail. It shows that both stator and rotor loss components have significant effect on the optimal split ratio and the machine performance. Moreover, as shown later, the selections of slot/pole combinations and magnet materials also affect the optimal split ratio notably. It should be noticed that the proposed simple analytical method is suitable for the initial design stage, and the influence of several loss components can hardly be considered, e.g. the PWM loss and the AC copper loss, etc. Since these losses highly depend on many factors, e.g.

the control method, the inverter switching frequency, the wire type and the displacement of coil, etc. In addition, these loss components can be also decreased by using several common techniques even in small high speed PM machines [20]-[22]. Consequently, these loss components are not considered in this paper, whereas their influence should be checked by using FE method in later design stages.

This paper is organized as follows. In Section II, various loss components are calculated, which includes stator iron loss, stator copper loss, windage loss and rotor eddy current loss. The output torque is determined analytically in Section III, and the optimal split ratio limited by different loss limitations is studied. Moreover, the influence of key design parameters, i.e. slot/pole combinations and magnet materials, is studied in Section IV. Finally, the FE analyses are carried out to validate the analytical predictions.

II. Loss Calculation

A. Stator loss calculation

Comparing with the low speed machine, the stator iron loss should be taken into account during the optimization in high speed machines due to the high frequency, which can significantly worsen the thermal condition and decrease the total efficiency.

The iron loss density can be estimated by [23]:

$$W_{fe} = k_h f B_{\max}^{\alpha} + k_c f^2 B_{\max}^2 + k_e f^{1.5} B_{\max}^{1.5} \quad (1)$$

where W_{fe} is the iron loss density, k_h, k_c and k_e are the hysteresis loss, eddy current loss and excess loss coefficients, respectively, f is the electrical frequency and $B_{\max}$ is the maximum stator flux density. In order to ease the investigation, a typical value of α is chosen, i.e. 2 [23].

As a result, the stator iron loss can be calculated by:

$$P_{fe} = W_{fe} m_{fe} \quad (2)$$

where P_{fe} is the stator iron loss and m_{fe} is the mass of stator iron which can be calculated by:

$$m_{fe} = A_{Fe} l_a \rho_{fe} = \left[\left(D_{so}^2 - D_{si}^2 \right) \pi / 4 - A_s N_s \right] l_a \rho_{fe} \quad (3)$$

where A_{fe} is the total stator iron area, l_a is the active length of machine, p_{fe} is the iron mass density, D_{so} and D_{si} are the outer and inner diameters of stator bore, A_s is the slot area and N_s denotes the number of slots.

The value of D_{si} can be calculated as

$$D_{si} = D_{so} \lambda + 2 \cdot \left(l_g + l_{sleeve} \right) \quad (4)$$

where l_g is the length of actual airgap, l_{sleeve} is the sleeve thickness and λ indicates the split ratio which is defined as

$$\lambda = D_{mo} / D_{so} \quad (5)$$

In (5), D_{mo} denotes the outer diameter of magnet. It should be noticed that D_{mo} is adopted in the definition of split ratio instead of actual rotor outer diameter. Although the sleeve thickness should also be considered as a part of the rotor outer diameter, non-magnetic materials are usually adopted for the sleeve, which indicates that the sleeve can be treated as an equivalent airgap in magnetic circuit. Consequently, D_{mo} is employed here to ease the investigation.

As for the slot area, it can be calculated as

$$A_s = \frac{\pi \cdot \left({D_{so}}^2 - \left(D_{si} + 2h_t \right)^2 \right)}{4N_s} - \frac{\pi \cdot {D_{so}}^2 - \pi \cdot \left(D_{so} - 2h_c \right)^2}{4N_s} - b_t \cdot \left(D_{so} / 2 - h_c - D_{si} / 2 - h_t \right) \quad (6)$$

where h_c, b_t, and h_t indicate the stator back-iron thickness, the stator tooth width and the tooth tip height, respectively.

For small high speed PM machines, a 2-pole rotor with diametric magnetization is usually used for the lowest electrical frequency. As a result, the airgap flux density is ideally sinusoidal. Consequently, the values of h_c and b_t can be determined as

$$b_t = k_a \cdot h_c = \frac{D_{ag}}{2} \cdot \frac{B_{g\max}}{B_{\max}} \cdot \int_{-\pi/N_s}^{\pi/N_s} \cos\theta d\theta \quad (7)$$

where k_a is the coefficient depending on the slot/pole combinations. It is 1 for the 6-slot/2-pole machine but 2 for the 3-slot/2-pole machine, D_{ag} is the diameter of middle of the equivalent airgap, and $B_{g\max}$ is the peak value of the airgap flux density.

In terms of the relationship between D_{ag} and D_{mo}, according to (4), it can be expressed as

$$D_{ag} = D_{mo} + l_g + l_{sleeve} \quad (8)$$

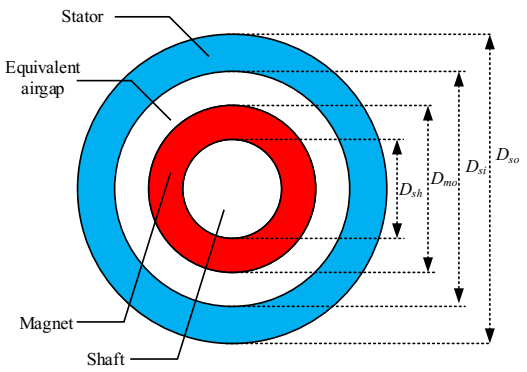

Fig. 1. Simplified motor model.

As for the peak value of airgap flux density, i.e. $B_{g\max}$, it can be determined analytically by

$$B_{g\max} = \frac{B_r}{2} \frac{1 - \left(D_{sh} / D_{mo} \right)^2}{1 - \left(D_1 / D_{si} \right)^2} \cdot \left[\left(D_{mo} / D_{si} \right)^2 + \left(D_{mo} / D_{ag} \right)^2 \right] \quad (9)$$

where D_{sh} is the outer diameter of shaft. B_r is the remanence of magnet, D_1 equals to D_{sh} when the shaft is magnetic and 0 when the shaft is nonmagnetic. It should be noticed that the motor is simplified as shown in Fig. 1, which indicates that the permeability of the soft magnetic material is assumed to be infinite and the influence of slot opening is neglected.

In addition to the stator iron loss, the stator copper loss should be calculated as well. It should be noticed that only DC copper loss is considered here, which indicates the proximity effect and the eddy current in windings are neglected.

As for the DC copper loss, its value can be expressed as

$$P_{cu} = 24 N_w^2 I_a^2 \rho \frac{\left(l_a + l_e \right)}{A_s K_s N_s} \quad (10)$$

where N_w is the number of turns per phase, I_a is the amplitude of

phase current, ρ is the resistivity of conductor, K_s is the filling factor and l_e denotes the length of the end winding .

In terms of the end winding length, it can be estimated by assuming the shape of end windings as the semi-circle [7] [8]. Therefore, the end winding length can be calculated as

$$l_e = \frac{\pi}{4}\left\{\left(\frac{D_{so}+D_{si}}{2}-h_c+h_t\right)\frac{\pi}{Ns}+b_t\right\} \tag{11}$$

As for the relationship between the copper loss and the stator iron loss, their sum should meet the stator thermal limitation.

In [3], [15], it is assumed that the temperature is evenly distributed in the stator, and all stator losses are transferred by convection. As a result, the maximum allowed stator loss, i.e. $P_{stator,\lim}$, can be roughly determined by the cooling capability of machines and calculated by

$$P_{stator,\lim} = h_{stator}\Delta\tau_{stator,\max}\pi D_{so} l_a \tag{12}$$

where $\Delta\tau_{stator,\max}$ is the maximum allowed stator temperature rise which mainly depends on the winding insulation class, h_{stator} indicates the stator overall heat transfer coefficient, its value usually ranges from 25W/(Km^2) to 100W/(Km^2) which depends on the cooling system [3].

As a result, the relationship between the copper loss and the stator iron loss can be expressed as

$$P_{stator,\lim} = P_{cu} + P_{fe} \tag{13}$$

B. Rotor loss calculation

In terms of rotor part, two loss components should be considered due to the high rotating frequency and the adoption of magnet ring, i.e. windage loss and rotor eddy current loss, respectively.

As for the windage loss, it can be calculated by [24]

$$P_{windage} = C_f \rho_{air}\pi\omega^3 r_{rotor}^4 l_a \tag{14}$$

where $P_{windage}$ indicates the windage loss, ρ_{air} is the air mass density, ω denotes the rotor angular velocity, r_{rotor} is the rotor outer radius including the sleeve thickness, and C_f is the friction coefficient which can be calculated as [24]

$$C_f = \frac{0.0152}{R_{e\delta}^{0.24}}\left[1+\left(\frac{8}{7}\right)^2\left(\frac{4R_{ea}}{R_{e\delta}}\right)^2\right]^{0.38} \tag{15}$$

where R_{ea} and $R_{e\delta}$ are the Reynolds number for an axial flow through the air gap and the Couette Reynolds number for the tangential flow forced by the rotating rotor and the turbulence. Their values can be expressed as

$$R_{e\delta} = \frac{\rho_{air}\omega r_{rotor} l_g}{\mu_{air}} \tag{16}$$

$$R_{ea} = \frac{\rho_{air} v_a 2 l_g}{\mu_{air}} \tag{17}$$

In (20) and (21), μ_{air} is the air dynamic viscosity and v_a indicates the axial speed of air.

In terms of the value of v_a, it can be roughly determined by

$$v_a = \frac{P_{rotor,\lim}}{C_a \cdot \Delta\tau_a \cdot A_a} \tag{18}$$

where $P_{rotor,\lim}$ is the maximum allowed rotor loss, as shown later, it mainly depends on the cooling capability in the airgap and the maximum allowed rotor size, C_a is the specific heat capacity of the coolant, $\Delta\tau_a$ is the variation of the coolant temperature and A_a is the area of the airgap cross section. It should be noticed that the value of v_a depends on $P_{rotor,\lim}$ in practice. However, in order to ease the investigation, v_a is kept the same in later studies, in which the value should be determined under the most critical rotor thermal situation.

As for the rotor eddy current loss, it can be determined analytically or by using FE method. The analytical solution is presented in detail in [25].

Similar to stator part, the sum of rotor loss components should meet the rotor thermal limitation as well. In small high speed machine, in order to keep the rotor temperature below the value which could demagnetize the magnet, the effective cooling in the airgap should be provided [26]. According to [27], the stator and rotor parts can be approximately treated as thermally isolated due to the effective airgap cooling, which means the rotor loss can be also limited by a similar equation to (12) as

$$P_{rotor,\lim} = h_{rotor}\Delta\tau_{rotor,\max}\pi D_{ro} l_a \tag{19}$$

where $P_{rotor,\lim}$ is the maximum allowed rotor loss, h_{rotor} is the rotor overall heat transfer coefficient decided by the cooling method, and $\Delta\tau_{rotor,\max}$ is the maximum allowed rotor temperature variation which depends on the magnet material significantly.

Consequently, the sum of the rotor eddy current loss and the windage loss is restricted by $P_{rotor,\lim}$, which can be expressed as

$$P_{rotor,\lim} = P_{rotor,eddy} + P_{windage} \tag{20}$$

where $P_{rotor,eddy}$ denotes the allowed rotor eddy current loss.

III. Torque Calculation

Before detailed torque calculations, the prototype machine will be introduced. The 6-slot/2-pole machine is chosen at first while the influence of slot/pole combinations will be investigated in later sections. The machine cross section is shown in Fig.2 and the detailed design parameters are listed in Table I. It should be noticed that this paper mainly focuses on the split ratio optimization considering different loss limitations. In order to simplify the investigation, a relative thick Inconel sleeve is employed for the prototype machine. The sleeve thickness is designed as 2mm in a machine with 215m/s surface speed in [28]. Since the maximum surface speed in the prototype machine in this paper is much lower, a 1mm Inconel sleeve is employed.

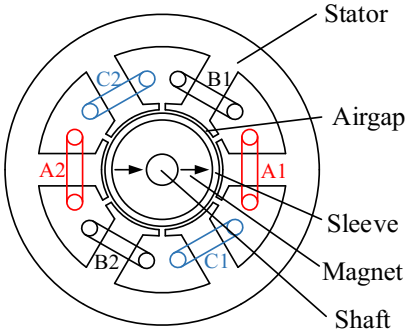

Fig. 2. Cross section of prototype machine.

TABLE I
DETAILED PARAMETERS OF PROTOTYPE MACHINE

Stator outer diameter (mm)	50	Sleeve thickness (mm)	1
Shaft diameter (mm)	5	Airgap length (mm)	1
Rotating speed (krpm)	110	Maximum stator loss (W)	25
Active length (mm)	12	Slot opening width (mm)	2
Tooth tip height (mm)	1	Filling factor	0.4
Sleeve material	Inconel	Maximum stator flux density (T)	1

In the prototype machine, the diametric magnetized magnet ring and the concentrated tooth-coil winding are employed. The magnet is chosen as NdFeB35UH at first and the influence of magnet materials will be investigated in later sections. The sleeve material is chosen as Inconel 718 whose thickness is fixed at1mm in the optimization process.

The output torque of a 3-phase machine with sinusoidal airgap flux density distribution under 120° electrical degree brushless DC operation can be expressed as [11]:

$$T = \frac{3\sqrt{3}}{\pi} N_w D_{ag} l_a K_{dp} I_a B_{g\max} \tag{21}$$

where T denotes the output torque and K_{dp} is the winding factor.

It should be noticed that the outer diameter of magnet is usually used for output torque calculation in large surface mounted PM machines, since the airgap length is usually much smaller than the rotor outer diameter. However, in small high speed PM machines, due to the relative large airgap length and the existence of retaining sleeve, the diameter of the middle of equivalent airgap should be used for more accurate calculation.

A. Torque considering stator loss limitation only

For the torque in model considering stator loss only, the phase current I_a should be calculated at first, which can be expressed as [7]

$$I_a = \frac{1}{N_w}\sqrt{\frac{P_{cu} A_s K_s N_s}{24\rho\left(l_a + l_e\right)}} \tag{22}$$

Consequently, the torque can be calculated as [15]

$$T = \frac{3\sqrt{3}}{\pi} D_{ag} l_a B_{g\max} K_{dp} \sqrt{\frac{\left(P_{stator,\lim} - P_{fe}\right) A_s K_s N_s}{24\rho\left(l_a + l_e\right)}} \tag{23}$$

The volume of the motor can be calculated as [7]

$$V = \frac{D_{so}^2 \pi \cdot l_a}{4} \tag{24}$$

As a result, the torque density is

$$T/V = C \cdot \left(\lambda + \frac{l_g + l_{sleeve}}{D_{so}}\right) B_{g\max} \sqrt{\frac{A_s}{l_a + l_e}} \cdot \sqrt{P_{stator,\lim} - P_{Fe}} \tag{25}$$

$$C = \frac{3K_{dp}}{\pi^2 D_{so}} \sqrt{\frac{2K_s N_s}{\rho}} \tag{26}$$

As can be seen, the torque density is a function of split ratio. Consequently, the optimal split ratio could be determined by solving the differential equation as

$$\frac{\partial\left(T/V\right)}{\partial\lambda} = 0 \tag{27}$$

The variation of output torque with split ratio in the model considering stator loss only is shown in Fig.3.

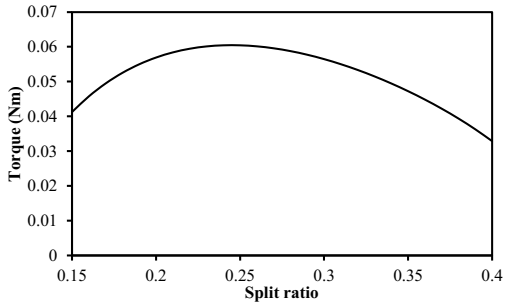

Fig. 3. Variation of torque with split ratio in model considering stator loss only.

As can be seen, there is an optimal split ratio when the stator loss is considered only. This is due to the fact that B_{gmax} increases with split ratio while the slot area represents an opposite trend as shown Fig. 4. As a result, the increased split ratio significantly increases the iron loss but decreases the copper loss as shown in Fig.5. Consequently, the phase ampere turns decreases with split ratio which is shown in Fig.6, and hence, the armature field.

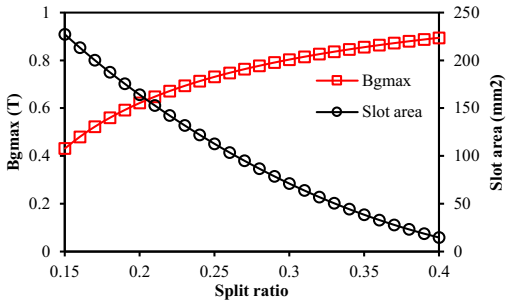

Fig. 4. Variation of B_{gmax} and A_s with split ratio in model considering stator loss only.

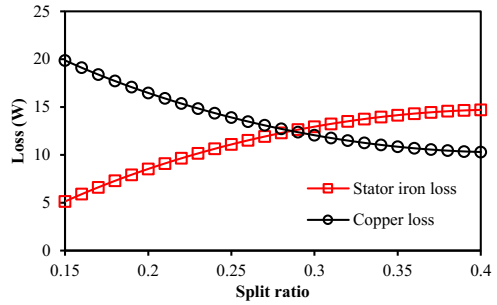

Fig. 5. Variation of stator loss components with split ratio in model considering stator loss only.

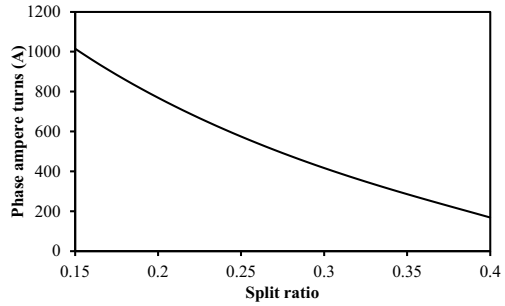

Fig. 6. Variation of phase ampere turns with split ratio in model considering stator loss only.

Accordingly, there should be an optimal split ratio which can balance the PM field and the armature field so that the maximum output torque can be obtained.

It should be noticed that the phase ampere turns are used here instead of phase current. As the number of turns per phase is related to many factors, i.e. slot area, diameter of wire, voltage limitation as well as parallel path, etc., which indicates that its value is hard to be determined at this design stage.

B. Torque considering rotor loss limitation only

When the torque is limited by the rotor loss only, the torque equation (23) can be also applied. Nevertheless, the current calculation should be determined by the rotor loss, and the influence of temperature on magnet properties, e.g. magnet remanence, should be taken into account.

As for the relationship between the phase current and the rotor loss, since the influence of slot opening and saturation is neglected, $P_{rotor,eddy}$ is determined by the phase current as well as the split ratio [25]. From another perspective, the phase current I_a limited by the $P_{rotor,eddy}$ can be determined when the split ratio is specified. Consequently, the phase current can be expressed as

$$I_a = f^{-1}\left(P_{rotor,eddy}\left(I_a,\lambda\right)\right) \tag{28}$$

As a consequence, the output torque is calculated as

$$T = \frac{3\sqrt{3}}{\pi} N_w D_{ag} l_a B_{g\max} K_{dp} f^{-1}\left(P_{rotor,eddy}\left(I_a,\lambda\right)\right) \tag{29}$$

As can be seen, when the rotor loss dominates the input current, the slot area is not shown in the output torque equation, which means it has no influence on the optimal split ratio.

In addition, temperature affects the magnet properties. As a result, the calculation of airgap flux density should take the influence of temperature into account, which can be expressed as

$$B_{g\max} = \frac{B_{r,temp}}{2}\frac{1-\left(D_{sh}/D_{mo}\right)^2}{1-\left(D_1/D_{si}\right)^2}\cdot\left[\left(D_{mo}/D_{si}\right)^2+\left(D_{mo}/D_{ag}\right)^2\right] \tag{30}$$

where $B_{r,temp}$ is the remanence with specific magnet temperature.

In this way, the variation of torque with different split ratio in the model only considering the rotor loss can be calculated, and the result is shown in Fig. 7.

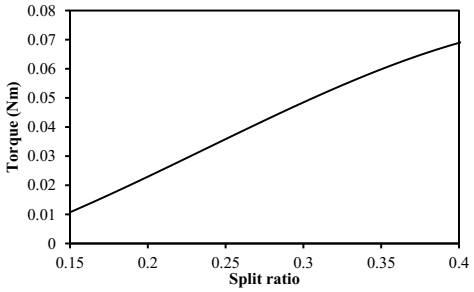

Fig. 7. Variation of torque with split ratio in model considering rotor loss only.

As shown, the output torque increases with split ratio monotonously. This is due to the fact that the allowed $P_{rotor,eddy}$ increases with split ratio shown in Fig. 8, which increases the phase ampere turns when the split ratio is small, and hence, the output torque.

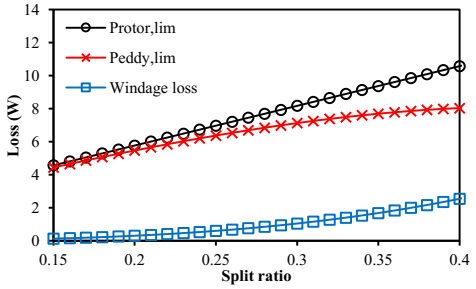

Fig. 8. Variation of rotor loss components with split ratio in model considering rotor loss only.

Although the value of phase ampere turns decreases slightly when the split ratio is relatively large as shown in Fig. 9, the torque still increases due to the enhancement of B_g and D_{ro} caused by increased split ratio.

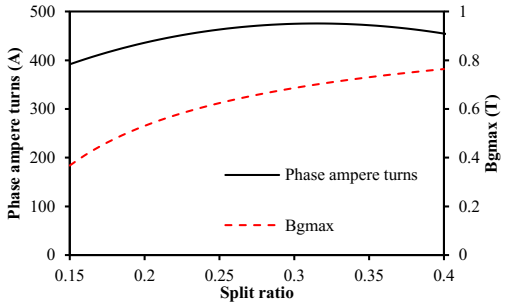

Fig. 9. Variation of phase ampere turns and B_g with split ratio in model considering rotor loss only.

C. Torque considering both stator and loss limitations

From the previous analyses, the variation of torque with split ratio represents very different behaviors when the limitations are different. In order to calculate the optimal split ratio and corresponding maximum output torque practically, both stator and rotor loss limitations should be considered simultaneously.

The variations of output torque and phase ampere turns with split ratio in the model considering both stator and rotor loss limitations are shown in Fig. 10.

It can be seen that two different regions can be divided. In region 1, the torque and current are limited by $P_{rotor,\lim}$, while in region 2, the torque and current are restrained by $P_{stator,\lim}$. Since different loss limitations are the main reason, the variations of different loss components with split ratio are calculated and shown Fig. 11, so that more details can be studied.

As shown in Fig. 11, the iron loss ascends with the split ratio all the time. In contrast, the copper loss increases with split ratio from a small value in region 1. In this region, the stator loss limitation can result in high value of phase ampere turns, which leads to unacceptable rotor loss.

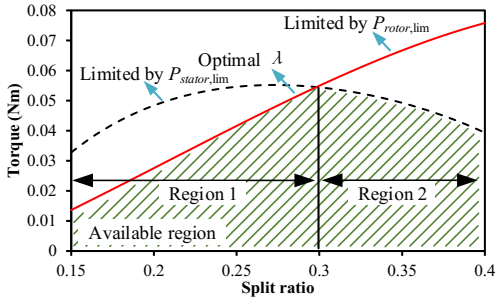

(a) Torque

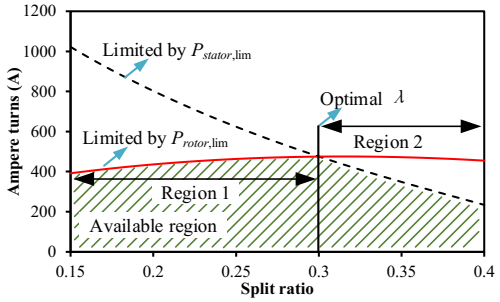

(b) Phase ampere turns

Fig. 10. Variation of torque and phase ampere turns in model considering both stator and rotor losses.

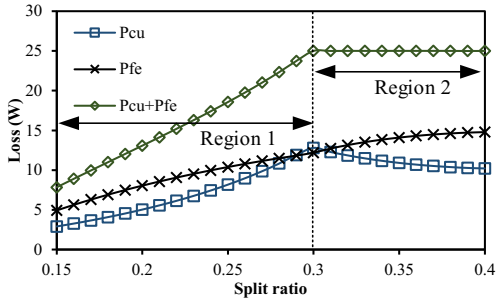

(a) Stator loss

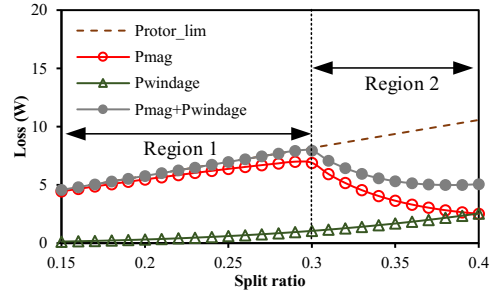

(b) Rotor loss

Fig. 11. Variation of stator and rotor loss components with split ratio in model considering both stator and rotor losses

As a result, the rotor loss limitation is more crucial for phase ampere turns in this region. Accordingly, the phase ampere turns increases with split ratio due to a higher allowed $P_{rotor,\lim}$, and it results in ascending copper loss as well as output torque.

With the increase of split ratio, $P_{rotor,\lim}$ ascends measurably according to (19), which results in significant increase of phase ampere turns. Meanwhile, the slot area decreases with split ratio. Consequently, the copper loss increases measurably. As a result, the sum of copper loss and stator iron loss reaches $P_{stator,\lim}$ at the beginning of region 2, and the phase ampere turns and output torque start to be restrained by stator loss limitation.

IV. Influence of Design Parameters

In previous sections, the optimal split ratio in small high speed PM machines is investigated. In this part, the influence of several key design parameters, e.g. slot/pole combinations and magnet materials will be studied in details.

A. Influence of slot/pole combinations

In previous investigations, the 6-slot/2-pole machine has been chosen as the prototype machine. Nevertheless, other possible slot/pole combinations can be competitive candidates for small high speed PM machines, e.g. 3-slot/2-pole, etc. Therefore, the influence of slot/pole combinations is studied here, and both 2-pole machines with 3 slots and 6 slots are considered. They share the same specifications listed in Table I.

The comparisons of rotor eddy current loss with split ratio and phase ampere-turns in machines having different slot/pole combinations are shown in Fig. 12.

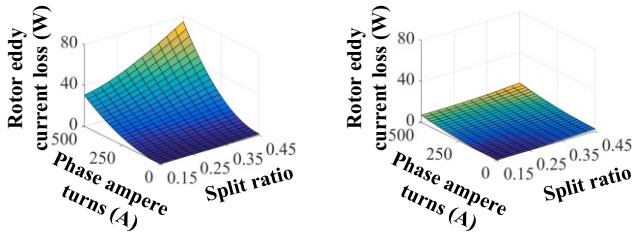

(a) 3-slot/2-pole (b) 6-slot/2-pole

Fig. 12. Variation of rotor eddy current loss with different phase ampere-turns and split ratio.

As can be seen, the 3-slot/2-pole machine has much larger rotor eddy current loss comparing with the 6-slot/2-pole machine when the phase ampere-turns and the split ratio are the same. This is due to the fact that there are abundant low-order even harmonics in airgap flux density of a 3-slot/2-pole machine, which is caused by the unbalanced winding structure and the asymmetric stator topology [29]. Consequently, the rotor eddy current loss should affect more significantly in the 3-slot/2-pole machine.

The variation of torque with split ratio in machines having different slot/pole combinations is shown in Fig. 13. It can be seen that the machine with 3-slot/2-pole has almost the same output torque but higher optimal split ratio comparing with the 6-slot/2-pole machine.

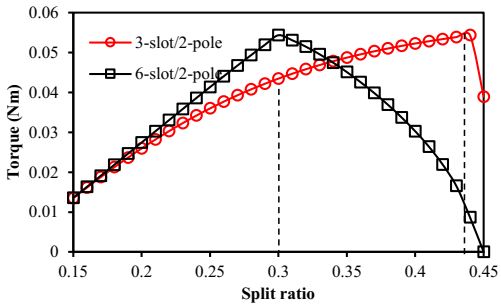

Fig. 13. Variation of torque with split ratio in machines with different slot/pole combinations.

To study in more details, the variations of loss components and phase ampere turns with split ratio are shown in Fig. 14.

As shown, rotor eddy current losses increase with the same track in both 3-slot/2-pole and 6-slot/2-pole machines when the split ratio is small. Since the rotor structure is the same in these two machines when the split ratio is specified, they have the same $P_{rotor,\lim}$ according to (19). However, since the 3-slot/2-pole machine has larger rotor eddy current loss shown in Fig. 12, it will have much smaller phase ampere turns at specific split ratio when $P_{rotor,\lim}$ is the limitation. In addition, the 3-slot/2-pole machine has relatively shorter total ending winding length but larger total slot area as shown in Fig. 15. As a result, the increase of copper loss will be relative slower in the 3-slot/2-pole machine. Therefore, $P_{stator,\lim}$ will restrain the

phase ampere turns at a larger split ratio in the 3-slot/2-pole machine, where the optimal split ratio occurs.

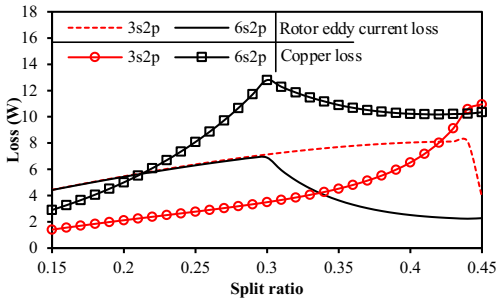

(a) Loss

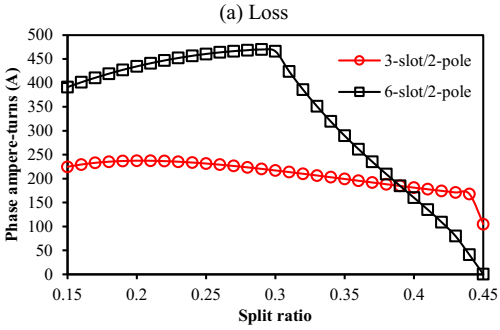

(b) Phase ampere turns

Fig. 14. Variation of loss and phase ampere turns with split ratio in machines with different slot/pole combinations.

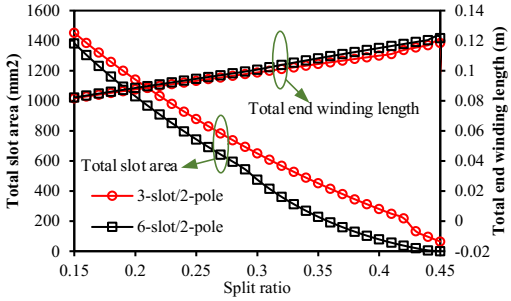

Fig. 15. Variation of total slot area and total ending length with split ratio in machines with different slot/pole combinations.

Meanwhile, due to low level of phase ampere turns but higher winding factor, i.e. 0.866 for 3-slot/2-pole but 0.5 for 6-slot/2-pole machines, and relative larger optimal split ratio, the maximum output torque of the 3-slot/2-pole machine has almost the same value comparing with the 6-slot/2-pole machine..

B. Influence of magnet material

In previous sections, the NdFeB35UH is chosen as the magnet material. However, the magnet material could be different according to applications, which can result in significant difference in terms of the machine performance. As a result, the influence of magnet materials on the optimal split ratio will be investigated in this section.

Two different permanent magnet materials are chosen, i.e. NdFeB35UH and SmCo Recoma18, respectively. Comparing with NdFeB35UH, SmCo Recoma 18 can provide much higher working temperature which is set as 150°C for NdFeB35UH but 250°C for SmCo Recoma 18. In addition, the variation of remanence with temperature is shown in Fig.16. As shown, the remanence of SmCo Recoma 18 is lower but less sensitive to temperature.

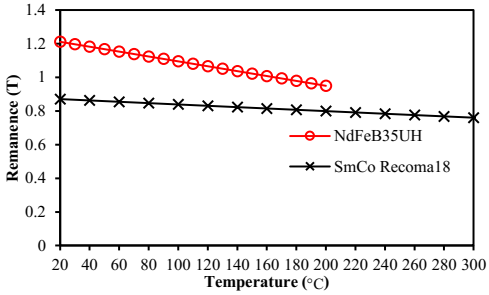

Fig. 16. Variation of magnet remanence with split ratio in machine with different magnet materials.

The variations of torque with split ratio in the machines having different magnet materials are shown in Fig.17. As can be seen, comparing with the machine having NdFeB35UH, the rotor loss has very limited influence on the optimal split ratio when the SmCo Recoma 18 is adopted. This is due to the fact that the torque starts to be limited by $P_{stator,\lim}$ before the optimal split ratio determined by $P_{stator,\lim}$ occurs.

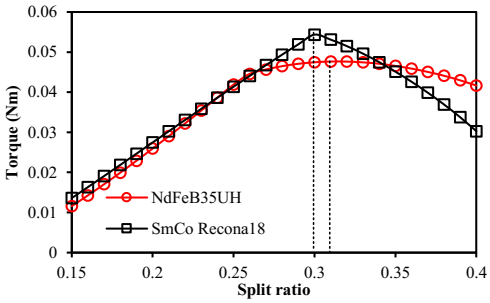

Fig. 17. Variation of torque with split ratio in machines with different magnet materials.

In order to explain in more details, the variation of loss with split ratio is investigated and shown in Fig. 18.

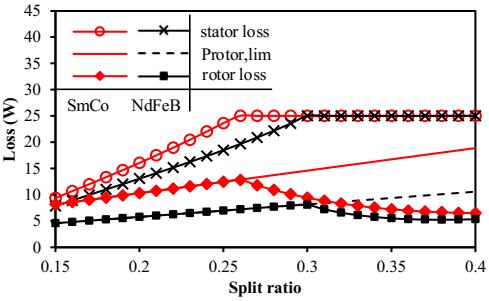

Fig. 18. Variation of loss with split ratio in machines with different magnet materials.

According to (19), the allowed rotor loss is much higher in machine with SmCo Recoma 18 due to the larger maximum allowed working temperature. In addition, since the rotor eddy current loss is determined by the phase ampere turns when the split ratio is fixed, the machine with SmCo Recoma 18 allows higher phase ampere turns with the specific split ratio in region 1, which also results in higher copper loss in machines with SmCo Recoma 18. Consequently, with the increase of phase ampere turns, $P_{stator,\lim}$ will restrain the phase ampere-turns in machines with Recoma 18 quickly due to the rapidly ascended copper loss, even before the optimal split ratio determined by $P_{stator,\lim}$ only occurs.

V. FE VALIDATION

The FE results are carried out in this section for validation. Both 3-slot/2-pole and 6-slot/2-pole machines considering stator and rotor loss limitations are considered, the detailed parameters are the same as shown in Table I, and NdFeB35UH is employed.

The variations of torque predicted by analytical and FE methods are calculated and shown in Fig. 19. Both linear and non-linear soft magnetic materials are considered, which are marked as circle and cross, respectively.

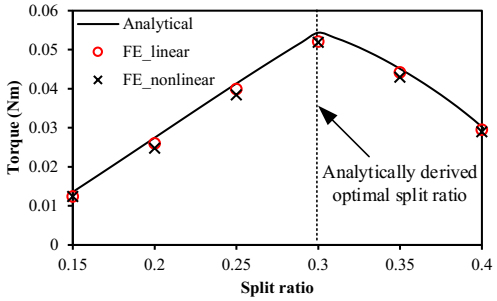

(a) 6-slot/2-pole

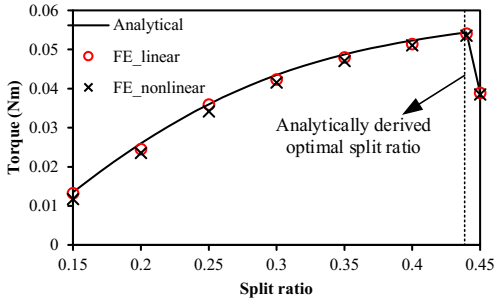

(b) 3-slot/2-pole

Fig. 19. FE validation of variation of torque with split ratio.

As shown, the difference between analytical and FE predictions is very small no matter the saturation is considered or not. This is due to the fact that B_{max} is typically chosen as a very small in high speed machine to avoid large iron loss. Consequently, the influence of saturation can be almost neglected.

VI. CONCLUSION

In this paper, a new analytical method is proposed to optimize the split ratio in small high speed PM machines. Copper loss, stator iron loss, windage loss and rotor eddy current loss have been considered. It shows that both stator and rotor loss components have significant influence on the machine performance and the optimal split ratio. By considering the rotor eddy current loss, the optimal split ratio may be increased significantly in certain situations. Moreover, the influence of slot/pole combinations and magnet materials has been investigated in details. It shows that the 3-slot/2-pole machine is affected more seriously by the rotor eddy current loss comparing with the 6-slot/2-pole machine. In addition, the rotor loss has less influence on the machine with SmCo Recoma18 comparing that with NdFeB35UH. Finally, FE results are carried out for validation, which show good agreement with the analytical predictions.

REFERENCES

[1] A. Binder and T. Schneider, "High-speed inverter-fed AC drives," in *Proc. ACEMP*, pp. 9-16, Sep. 2007.

[2] D. Gerada, A. Mebarki, N. L. Brown, C. Gerada, A. Cavagnino, and A. Boglietti, "High-speed electrical machines: technologies, trends, and developments," *IEEE Trans. Ind. Electron.*, vol. 61, no. 6, pp. 2946-2959, Jun. 2014.

[3] N. Bianchi, S. Bolognani, and F. Luise, "Potentials and limits of high speed PM motors," *IEEE Trans. Ind. Appl.*, vol. 40, no. 6, pp. 1570–1578, Nov. 2004.

[4] A. Tenconi, S. Vaschetto, and A. Vigliani, "Electrical machines for high-speed applications: design considerations and tradeoffs," *IEEE Trans. Ind. Electron.*, vol. 61, no. 6, pp.3022-3029, Jun. 2014.

[5] Chenjum Cui, Gang Liu, Kun Wang, and Xinda Song, "Sensorless drive for high-speed brushless DC motor based on the virtual neutral voltage," *IEEE Trans. Power Electro.,* vol. 30, no. 6, pp. 3275-3285, Jun. 2015.

[6] Hesmondhalgh, D.E., Tipping, D., and Amrani, M.: "Design and construction of a high-speed high-performance direct-drive handpiece", *IEE Proc. B Electr. Power Appl.,* 134, (6), pp. 286–296. 1987.

[7] Y. Pang, Z. Q. Zhu, and D. Howe, "Analytical determination of optimal split ratio for permanent magnet brushless motors", *IEE Proceedings Electric Power Appl.*, vol. 153, no. 1, pp. 7-13, 2006.

[8] Y. Shen, and Z. Q. Zhu, "Analytical prediction of optimal split ratio for fractional-slot external rotor PM brushless machines", *IEEE Trans. Magn.,* vol. 47, no. 10, pp. 4187-4190, Oct. 2011.

[9] W. Q. Chu, Z. Q. Zhu, "Optimal split ratio and torque comparison of surface-mounted permanent magnet machines having inner or outer rotor", *in Proc.6th IET Int. Conf. on Power Electr., Machines and Drives,* Bristol, U.K, pp. 1-6, Mar, 2012.

[10] L. J. Wu, Z. Q. Zhu, J. T. Chen, Z. P. Xia, and G. W. Jewell, "Optimal split ratio in fractional-slot interior permanent-magnet machines with non-overlapping windings", *IEEE Transactions on Magnetics,* vol. 46, no. 5, pp. 1235-1242, 2009.

[11] J. D. Ede, Z. Q. Zhu, and D. Howe, "Optimal split ratio for high-speed permanent magnet brushless DC motors", *International Conference on Electrical Machines and Systems,* vol. 2, pp. 909-912, 2001.

[12] Z. Q. Zhu, K. Ng, and D. Howe, "Design and analysis of high-speed brushless permanent magnet," in *Proc. of Electrical Machines and Drives (EMD) Conf.*, pp. 381–385, Sep. 1–3, 1997.

[13] X. G. Fan, R. H. Qu, B. Zhang, J. Li, and D. W. Li, "Split ratio optimization of high-speed permanent magnet synchronous machines based on thermal resistance network," *Int. Conf. on Electr. Machines,* Sept. 2016.

[14] Q. W. Li, M. F. Dou, C. Fang, "Analytical determination of optimal split ratio for high speed permanent magnet brushless motors," *Int. Conf. on Electrical Machines and Systems (ICEMS)*, Oct. 2015.

[15] Y. Wang, J. H. Feng, S. Y. Guo, Y. F. Li, Z. C. Chen, Y. Wang, and Z. Q. Zhu, "Investigation of optimal split ratio for high-speed permanent magnet brushless machines," *IEEE Trans. Magn*., vol. 54, no. 11, article sequence number: 8105605, 2018.

[16] T. Wang, F. Wang, H. Bai, and J. Xing, "Optimization design of rotor structure for high speed permanent magnet machines," *in Proc. Int. Conf. Elect. Mach. Syst.*, Seoul, Korea, Oct. 8–11, 2007, pp. 1438–1442.

[17] N. Bianchi, S. Bolognani, and Fabio Luise, "Analysis and design of a PM brushless motor for high speed operations", *IEEE Transactions on Energy Conversion*, vol. 20, no. 3, pp.629-637, 2005.

[18] S. Xu, X. Liu, and Y. Le, "Electromagnetic design of a high speed solid cylindrical permanent-magnet motor equipped with active magnetic bearings," *IEEE Trans. Magn.*, vol. 53, no. 8, Apr. 2017, Art. no. 8203715.

[19] D. Ions, and D. M. Jones, "Rotor for an electrical machine," U.S. Patent 8756794, June 24 2014.

[20] R. Liu, C. C. Mi, and D. W. Gao, "Modeling of eddy-current loss of electrical machines and transformers operated by pulse width modulated inverters," *IEEE Trans. Magn.,* vol. 44, pp. 2021-2028, Aug. 2008.

[21] C. J. Cui, G. Liu, K. Wang, and X. D. Song, "Sensorless drive for high speed brushless DC motor based on the virtual neutral voltage," IEEE *Trans. Power Electron.*, vol. 30, no. 6, pp. 3275-3285, Jun. 2015.

[22] D. A. Gonzalez, D. M. Saban, "Study of the copper losses in a high-speed permanent-magnet machine with form-wound windings," *IEEE Trans.*

Ind. Electron, vol. 61, no. 6, pp. 3038-3045, 2014.

[23] D. M. Ionel, M. Popescu, M. I. McGilp, T. J. E. Miller, S. J. Dellinger, and R. J. Heideman, "Computation of core losses in electrical machines using improved models for laminated steel," *IEEE Trans. Ind. Appl.*, vol. 43, no. 6, pp. 1554–1564, Nov. 2007.

[24] Y. Yamada, "Torque resistance of a flow between rotating co-axial cylinders having axial flow," *Bulletin of Japan Society of Mechanical Engineers (JSME)*, vol. 5, no. 20, pp. 634-642. 1962.

[25] Z. Zhu, K. Ng, N. Schofield, and D. Howe, "Improved analytical modelling of rotor eddy current loss in brushless machines equipped with surface-mounted permanent magnets," *IEE Proceedings Electric Power Applications*, vol. 151, no. 6, pp. 641–650, Nov. 2004.

[26] O. Aglen, "Loss calculation and thermal analysis of a high-speed generator," *IEEE IEMDC conference*, pp. 1117-1123, Jun. 2003.

[27] J. Dong, Y. K. Huang, L. Jin, B. C. Guo, H. Y. Lin, J. Y. Dong, M. Cheng, and H. Yang, "Electromagnetic and thermal analysis of open-circuit air cooled high-speed permanent magnet machines with gramme ring windings," *IEEE Trans. Magn.*, vol. 50, no. 11, pp. 1–4, Nov. 2014.

[28] Y. Wang, J. H. Feng, S. Y. Guo, Y. F. Li, Z. C. Chen, Y. Wang, and Z. Q. Zhu, "Investigation of optimal split ratio for high speed permanent magnet brushless machines," *IEEE Trans. Magn.*, vol. 54, no. 11, article sequence number: 8105605, 2018.

[29] J. Ma, and Z. Q. Zhu, "Magnet eddy current loss reduction in permanent magnet machines," *IEEE Trans. Ind. Appl*., early access, pp. 1-1. 2018.

Jie Ma was born in Shanxi, China, in 1992. He received the M.Sc. degree in electronic and electrical engineering from the University of Sheffield, Sheffield, U.K., in 2015. He is currently working toward the Ph.D. degree at the University of Sheffield, Sheffield, U.K.

His major research interests include the design and analysis of high speed permanent magnet machines

Z. Q. Zhu received the B.Eng. and M.Sc. degrees from Zhejiang University, Hangzhou, China, in 1982 and 1984, respectively, and the Ph.D. degree from the University of Sheffield, Sheffield, U.K., in 1991, all in electrical engineering.

Since 1988, he has been with the University of Sheffield, where since 2000, he has been a Professor with the Department of Electronic and Electrical Engineering. He is currently the Royal Academy of Engineering/Siemens Research Chair, and the Head of the Electrical Machines and Drives Research Group, the Academic Director of Sheffield Siemens Wind Power Research Centre, the Director of CRRC Electric Drives Technology Research Centre, and the Director of Midea Electric Machines and Controls Research Centre. His current major research interests include the design and control of permanent magnet brushless machines and drives for applications ranging from electric vehicles through domestic appliance to renewable energy. He is a Fellow of Royal Academy of Engineering, U.K., a Fellow of Institute of Electrical and Electronics Engineers, U.S.A., and a Fellow of Institute of Engineering and Technology (IET), U.K.